Force-velocity relation for growing biopolymers

A. E. Carlsson
Department of Physics, Washington University, St. Louis, Missouri 63130-4899
(Received 1 March 2000; revised manuscript received 10 July 2000)

The process of force generation by the growth of biopolymers is simulated via a Langevin-dynamics approach. The monomer-monomer interaction forces are taken to have simple forms that favor the growth of straight fibers from solution, and they are taken to grow against a flat obstacle. The force-velocity relation is obtained from the simulations for two versions of the monomer-monomer force field. We evaluate corrections to the simplest analytic theory based on thermal motion of the obstacle, which yields an exponential velocity decay with applied force. For most orientations of the growing fiber tip, the corrections are small. However, for orientations in which the surface of the growing fiber is parallel to the obstacle, large corrections are obtained in the direction of reduced fiber velocity. These results are explained on the basis of the diffusion properties of monomers near the fiber tip. It is also found that the mobility of the obstacle has little effect on the growth rate over a broad range of possible values.

PACS number(s): 87.15.Rn, 87.16.Ac, 87.17.Jj

I. INTRODUCTION

The growth of biopolymers is a key ingredient in the crawling motion and internal transport processes of almost all eukaryotic cells. They crawl among each other and over substrates by motion of the cytoplasm into protrusions known as lamellipodia, filopodia, or microspikes according to their shapes. The forces driving the extension of these protusions are believed to come from the growth of a collection of fibers assembled from monomers of the protein actin. The actin fibers are approximately 7 nm in diameter. With no opposing force, they can grow at velocities [1] of over 1 μm/sec at physiological actin concentrations [2,3] of 10–50 μM; the velocities of the cell protrusions are typically [4,5] in the range of 0.1 μm/sec. Actin fiber growth also can power the motion of bacteria and viruses through the cell cytoplasm. The velocities usually range from 0.02 to 0.2 μm/sec, but velocities up to 1.5 μm/sec have been observed. As they move, they leave behind ''comet tails'' made up of actin fibers [6,7]. Recent experiments have studied the minimal ingredients necessary for such propulsion. For example, Ref. [8] shows that polystyrene beads coated with a catalytic agent for actin polymerization spontaneously move in cell extracts at velocities of 0.01 to 0.05 μm/sec, forming comet tails similar to those caused by bacteria and viruses. It has also been shown recently [9] that *Listeria* and *Shigella* bacteria can move in a medium much simpler than a cell extract, containing in addition to actin monomers only the proteins Arp2/3 complex, actin depolymerizing factor, and capping protein. In particular, myosin-type motors are not necessary for motion driven by actin polymerization. The minimal ingredients lead to velocities of 0.01 to 0.02 μm/sec; supplementation of this mix with other ingredients including profilin, α-actinin, and the vasodilator-stimulated phosphoprotein (VASP) protein increases the velocities up to 0.05 μm/sec. To our knowledge, there have been no measurements of the force-velocity relation for growing actin filaments. However, recent measurements of the actin fiber density [10] and Young's modulus [11] at the leading edge of lamellipodia would suggest forces on the order of 1 pN per fiber if all fibers are contributing equally; this is roughly equal to the basic force unit for fiber growth, kT/a, where k is Boltzmann's constant, T is temperature, and $a=2.7$ nm is the incremental fiber length per added monomer.

Microtubules, which are thicker fibers (22 nm) assembled from tubulin subunits, also exert forces when they grow. Microtubule assembly and disassembly is crucial in intracellular processes such as mitosis, the formation of cilia and flagella, and the transport of nutrients across the cell. Recent measurements [12] on microtubules *in vitro* have yielded explicit force-velocity curves. At zero force, the velocity is about 0.02 μm/sec; with increasing force, the velocity drops off roughly exponentially.

It is clear that growth of the fiber against a force results in a lowering of the system's free energy if the opposing force is sufficiently small, since the exothermic contribution from the attachment of monomers at the end of the polymer will outweigh the work done to move the obstacle against the external force. The critical force at which polymerization stops is determined by the balance of these two contributions. However, it is not yet understood in detail what factors determine the rate of growth and the maximum force at which a useful speed can be obtained. The basic difficulty of the polymer's growth process is that when the obstacle impinges directly on the fiber tip, there is not enough room for a new monomer to move in. Thus the rate of growth must be connected to the fluctuations of either the obstacle or the filament tip, which create temporary gaps between the tip and the obstacle. This effect has been treated explicitly in the ''thermal ratchet'' model [13]. In this model one assumes that the obstacle must be a critical distance a from the tip for growth to occur. The fiber is assumed to be rigid. The growth rate is obtained by a solution of a drift-diffusion-type equation. For conditions of slow growth, i.e., in which the time to add a monomer is much longer than the time it takes the obstacle to diffuse a distance a, this equation can be solved analytically. The forward growth rate is proportional to the probability that the obstacle-tip separation exceeds a. If depolymerization is sufficiently slow to be ignored, this yields the following dependence of the velocity v on the opposing force F:

$$v \propto \exp(-Fa/kT), \tag{1}$$

where k is Boltzmann's constant and T is the temperature. This result is equivalent to application of the principle of detailed balance [14], on the assumption that the depolymerization rate is independent of the opposing force. This work has been extended to flexible fibers at nonperpendicular incidence [15,16], and to interacting systems of fibers [17]. For flexible fibers, it is again found that the velocity is proportional to the probability forming of a gap large enough to admit the next monomer.

It is the purpose of this paper to evaluate the force-velocity relation for growing fibers using a model more realistic than those used previously. The model used to derive Eq. (1) does not explicitly treat the diffusion of monomers to the filament tip, but treats only the diffusive behavior of the variable describing the distance between the obstacle and the tip. It is assumed that once this distance exceeds a that the monomers can enter with a fixed probability independent of the tip-obstacle distance. This assumption needs to be evaluated by explicit treatment of the diffusion of the monomers. In addition, although the form of Eq. (1) is confirmed by the force-velocity relation for microtubules [12] the decay rate of the velocity with applied force was about twice as large as expected from Eq. (1). One possible explanation of this, suggested by Mogilner and Oster [17], is subsidy effects between the 13 fibers comprising a microtubule ''protofilament.'' We intend to investigate the extent to which other mechanisms can account for such discrepancies.

II. MODEL

Our model system contains a fiber of protein monomers growing against a flat rigid obstacle in two dimensions, at an angle θ_i relative to the obstacle's normal vector. We will be mainly interested in the actin system, but the basic physics of our results is relevant to any fiber growing against an obstacle. Our choice of two dimensions is dictated mainly by computational practicality: the simulations took over two weeks of CPU time on a Compaq 21264 processor and our preliminary studies indicate that the three-dimensional simulations take about 30 times longer. The fundamental units of the simulation are the monomers; their internal and rotational degrees of freedom are assumed to be included in our effective interaction energies. The motions of the monomers and the obstacle are treated via Langevin dynamics. The z direction is taken as the growth axis, with the obstacle parallel to the x direction. The coordinates of the monomer centers of mass are given by $\vec{r}_i$, and the z-coordinate of the obstacle is called Z. The Langevin equations for this system are $\mu_i^{-1} d\vec{r}_i/dt = \vec{F}_i + \vec{f}_i(t)$ for the monomers and $\mu_O^{-1} dZ_O/dt = F_O + f_O(t)$ for the obstacle, where the μ's are mobilities, F denotes deterministic interaction forces, and $\vec{f}_i$ and and f_O are random forces satisfying

$$\langle f_i^x(t) f_j^x(t') \rangle = \langle f_i^z(t) f_j^z(t') \rangle = 2\mu_i^{-1} kT \delta_{ij} \delta(t-t'), \tag{2}$$

$$\langle f_i^x(t) f_j^z(t') \rangle = 0, \tag{3}$$

and

$$\langle f_O(t) f_O(t') \rangle = 2\mu_O^{-1} kT \delta(t-t'). \tag{4}$$

The Langevin equations are implemented with a finite time step Δt following the procedure of Ref. [18]:

$$\vec{r}_i(t+\Delta t) = \vec{r}_i(t) + \Delta t \mu_i \vec{F}_i(t) + \vec{g}(t)\sqrt{kT\mu_i}, \tag{5}$$

and

$$Z(t+\Delta t) = Z(t) + \Delta t \mu_O \vec{F}_O(t) + h(t)\sqrt{kT\mu_O}, \tag{6}$$

where $\vec{g}(t)$ and $h(t)$ are random functions with zero time average, satisfying

$$\langle g^x(t) g^x(t') \rangle = \langle g^z(t) g^z(t') \rangle = \langle h(t) h(t') \rangle = 2\Delta t \delta_{tt'}. \tag{7}$$

To implement the last set of correlations, at each time step we choose h from a uniform random distribution between $-\sqrt{6\Delta t}$ to $\sqrt{6\Delta t}$, and $\vec{g}$ from a disk of radius $\sqrt{8\Delta t}$.

Since all of the monomers, including those in fiber, are allowed to move in the simulations, this simulation approach treats explicitly both the diffusion effects around the fiber tip and the fluctuations in the shape of the fiber and the position of the tip relative to the obstacle.

A. Force laws

The obstacle experiences an external force of magnitude F_{ext} in the $-z$ direction. In the absence of reliable force fields for the monomer-monomer interactions, we use a simple model form for the interactions which has a linear filament as the lowest-energy structure. This form contains two-body and three-body interactions. The two-body interactions are repulsive and have the form

$$V_2(r_{ij}) = V^{\text{rep}} \exp[-\kappa_{\text{rep}}(r_{ij}-a)]; \tag{8}$$

the three-body interaction energy has the form

$$V_3(\vec{r}_{ij}, \vec{r}_{ik}) = V^{\text{att}} \exp[-\kappa_{\text{att}}(r_{ij}-a)] \times \exp[-\kappa_{\text{att}}(r_{ik}-a)](\alpha + \cos\theta_{ij}), \tag{9}$$

with $0 < \alpha < 1$. It is attractive for $\theta_{ij} > \cos^{-1}(-\alpha)$. The monomer-obstacle interactions have only a two-body repulsive component, and have the form

$$W_2(z_i) = V^{\text{obst}} \exp[-\kappa_{\text{obst}} | z_i - (Z-a) |]. \tag{10}$$

The forces are obtained as gradients of these energy terms. The energies are modified by the subtraction of appropriate constants to force the interaction energy to go to zero at a cutoff distance $r_{\max}$ (in the case of the three-body terms this means that the energy vanishes if either r_{ij} or r_{ik} becomes greater than $r_{\max}$).

We use two parameter sets, whose values are given in Table I. These two parameter sets are chosen mainly to sample different shapes of the ''basin of attraction'' for the addition of a monomer, and by no means exhaustively sample the range of possible model force fields. The first corresponds to a narrow basin of attraction. The large value of α means that the three-body terms are positive only for a small range of angles. This is partly compensated for by the

TABLE I. Parameters used in simulations. Energies are given in units of kT, κ parameters in units of a^{-1}, and r_{max} in units of a, the equilibrium monomer spacing.

Force field	V_{rep}	V_{att}	V_{obst}	κ_{rep}	κ_{att}	κ_{obst}	α	r_{max}
Hard	141.3	6510	19.14	8.267	4.960	4.960	0.940	1.412
Soft	257.5	2151	27.44	7.666	4.600	4.600	0.770	1.522

choice of prefactors to avoid the binding energy becoming too small. We will call this the ''hard'' force field. The corresponding energy contours are shown in Fig. 1(a). The radius of the basin of attraction, or the region over which the force pulls the next monomer into its minimum-energy position, is about a tenth the size of a monomer, which would correspond to a few angstroms for actin monomers. Figure 1(b) shows the energy contours for the parameters corresponding to a wider basin of attraction, which is about half the size of a monomer. We call this the ''soft'' force field. For both of the force fields, the binding energies are very large compared to kT, so that monomer subtraction from the fiber does not occur in the simulations. This is a reasonable approximation; from the measured on and off constants in Ref. [1], the ratio of on to off rates at physiological actin monomer concentrations would be less than 0.01. We feel that the ''hard'' force field is more physically significant since its persistence length is 2650 monomers, which would correspond to 7.2 μm for actin, in comparison with the experimental value [19] of about 7 μm; that for the ''soft'' force field is 3.7 μm.

With regard to the mobilities, the only physically relevant factor is the ratio of the obstacle mobility to the monomer mobility, since multiplicative changes in all the mobilities simply serve to scale up the fiber growth velocities; these will thus factor out of our velocity results, which are scaled by $1/\mu kT$. For most of our simulations we use a mobility of the obstacle equal to that of the monomers for simplicity. This would correspond to identifying the obstacle with a part of a fluctuating membrane rather than an entire rigid particle. We have varied the obstacle mobility in a few cases, with results to be discussed below.

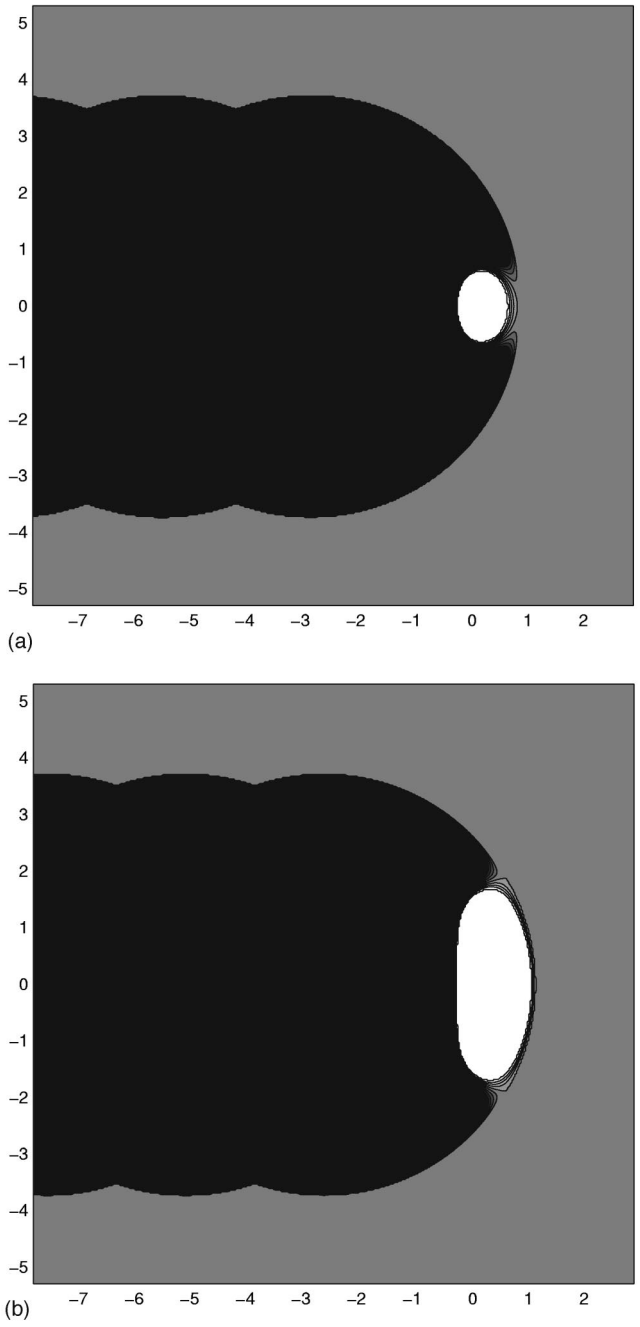

FIG. 1. Energy contours for a monomer approaching a fiber tip with hard (a) and soft (b) force fields. Contour heights correspond to integer multiples of kT, with lighter corresponding to lower energies. The length units are nm, assuming a monomer step size of 2.7 nm as for actin.

B. Filament-growth procedure

A typical physiological concentration of actin (10 μM) is low in the sense that the average spacing between actin monomers is about 60 nm, roughly ten times the monomer size. This means that the probability that two free monomers are near enough to interact with each other is very small. For this reason we adopt a growth procedure in which only one free monomer at a time interacts with the tip. This is accomplished as follows. We start with a fiber of six monomers pointing in the z direction at their equilibrium spacing. A free monomer is then added at a point on a circle of radius R centered on the next attachment site [20] (defined as one monomer spacing beyond the monomer at the fiber tip). We choose $R=2.5a$, which places the added monomer well beyond the interaction range of the monomer at the tip. The relative probabilities of monomer addition at different points on the circle are proportional to $\exp[-W_2(z)/kT]$. This weighting is accomplished by choosing a random number for each potential addition point; if this random number is less than $\exp[-W_2(z)/kT]$, then this point is rejected and another one is chosen. A new point is also chosen if the monomer overlaps the fiber (i.e., its distance to the fiber is less than r_{max}). The system is then stepped forward in time according to the procedure described above, until one of two possible termination events occur:

(1) The monomer diffuses outside of the R circle. In this case it is restarted on the circle as above. If the obstacle abuts the fiber, the position of the monomer is constrained to be

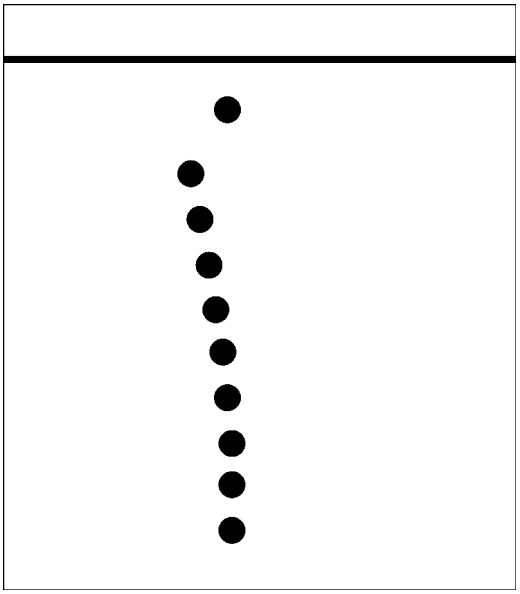

FIG. 2. Typical fiber-obstacle configuration during simulations.

out of the interaction range of the obstacle.

(2) The monomer attaches to the tip. In this case, another monomer is started on the R circle.

In this way, the CPU time that is used in the simulation is focused on the time that the monomers spend close to the tip. A snapshot of a typical simulation configuration in the perpendicular incidence case ($\theta_i = 0$) is shown in Fig. 2.

One can use the computed growth rates to predict growth rates for low concentrations c, by multiplying the computed rates by the probability $P(c)$ of finding a monomer inside the R circle. We obtain this probability numerically as

$$P(c) = \frac{1}{c}\int_{r<R} \exp[-U(\vec{r})/kT]d^2r, \tag{11}$$

where $U(\vec{r})$ is the energy (from both fiber and obstacle) associated with placing a monomer at the point $\vec{r}$, and the coordinates are given with respect to the next attachment point [21]. Points in the basin of attraction (negative U) are excluded from the integral. We plot our force-velocity relations in terms of the force acting between the obstacle and the fiber tip. This exceeds the external force applied on the obstacle by an amount corresponding to the viscous drag on the obstacle as it moves through the medium. The total force is thus given as $F = F_{\text{ext}} + v/\mu_O$.

III. RESULTS

Our simulations involve ten runs, each of which involves the addition of 30 monomers to the fiber tip. This corresponds to a statistical uncertainty of $\sqrt{1/300} = 6\%$ in the growth velocities. Typical results for the fiber length as a function of time are shown in Fig. 3. Note that there are no backwards steps because the parameters that are used in the force field result in an exothermic enthalpy for monomer addition that exceeds kT by at least a factor of 20. We use a concentration corresponding to one monomer per square of side $20a$; in our model, velocities at other concentrations would be given by a linear proportionality.

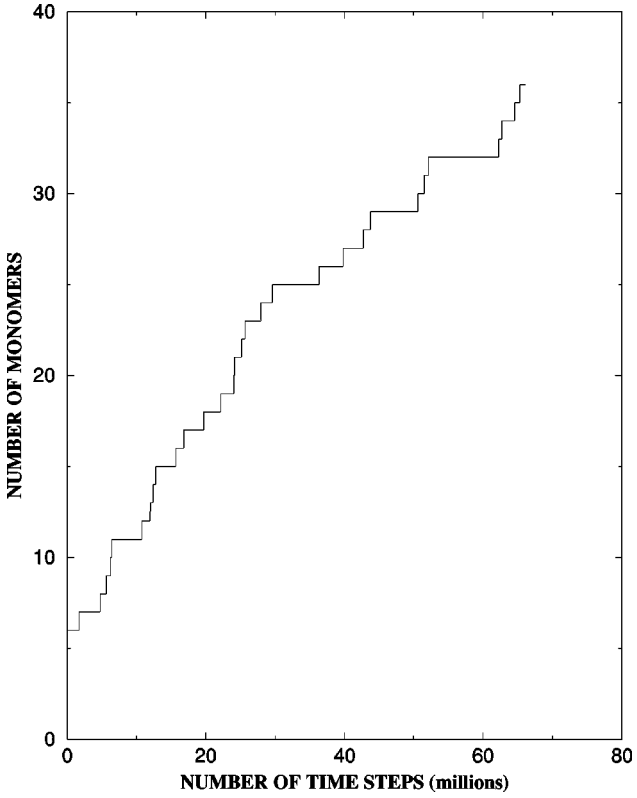

FIG. 3. Representative plot of the number of monomers in fiber vs the number of time steps. Obtained for $Fa/kT = 1.5$, $\theta_i = 0$, and the hard force field.

A. Force-velocity relation

Figure 4(a) shows growth velocity (solid circles) vs applied force for the hard force field [cf. Fig. 1(a)] at perpendicular incidence. For comparison, a curve proportional to $\exp(-Fa/kT)$ is shown. The simulation results give noticeably lower velocities at finite applied forces than the exponential prediction. The discrepancy is about 65% at $Fa/kT = 1$, and 85% at $Fa/kT = 2.5$. The results can be roughly fitted to a different exponential curve, of the form $\exp(-1.7Fa/kT)$. Thus the growth velocity is much more sensitive to force than the thermal-ratchet model would predict. Figure 4(b) shows similar results for the soft force field [cf. Fig. 1(b)], again for perpendicular incidence. The free-fiber growth velocity is about twice that for the hard force field because the attraction basin is larger. The discrepancies between the simulation results and the analytic theory are comparable to those seen for the hard force field, but somewhat less pronounced. The discrepancy at $Fa/kT = 2.5$ is 70%, and the exponential fit curve is $\exp(-1.5Fa/kT)$. The open diamonds in Fig. 4(a) correspond to the results of varying the mobility μ_O; for the leftmost one the mobility is doubled, and for the rightmost one it is reduced by a factor of 10. The effects of these variations are very minor, as predicted by the ''thermal-ratchet'' model [13].

Figure 4(c) shows results for oblique incidence, using $\theta_i = 45°$ and the hard force field. Because of phase space considerations, we expect these results to be more typical of an average growing fiber than those for $\theta_i = 0$. The quantity plotted on the horizontal axis is the vertical force; the component projected on the fiber growth direction is smaller by a

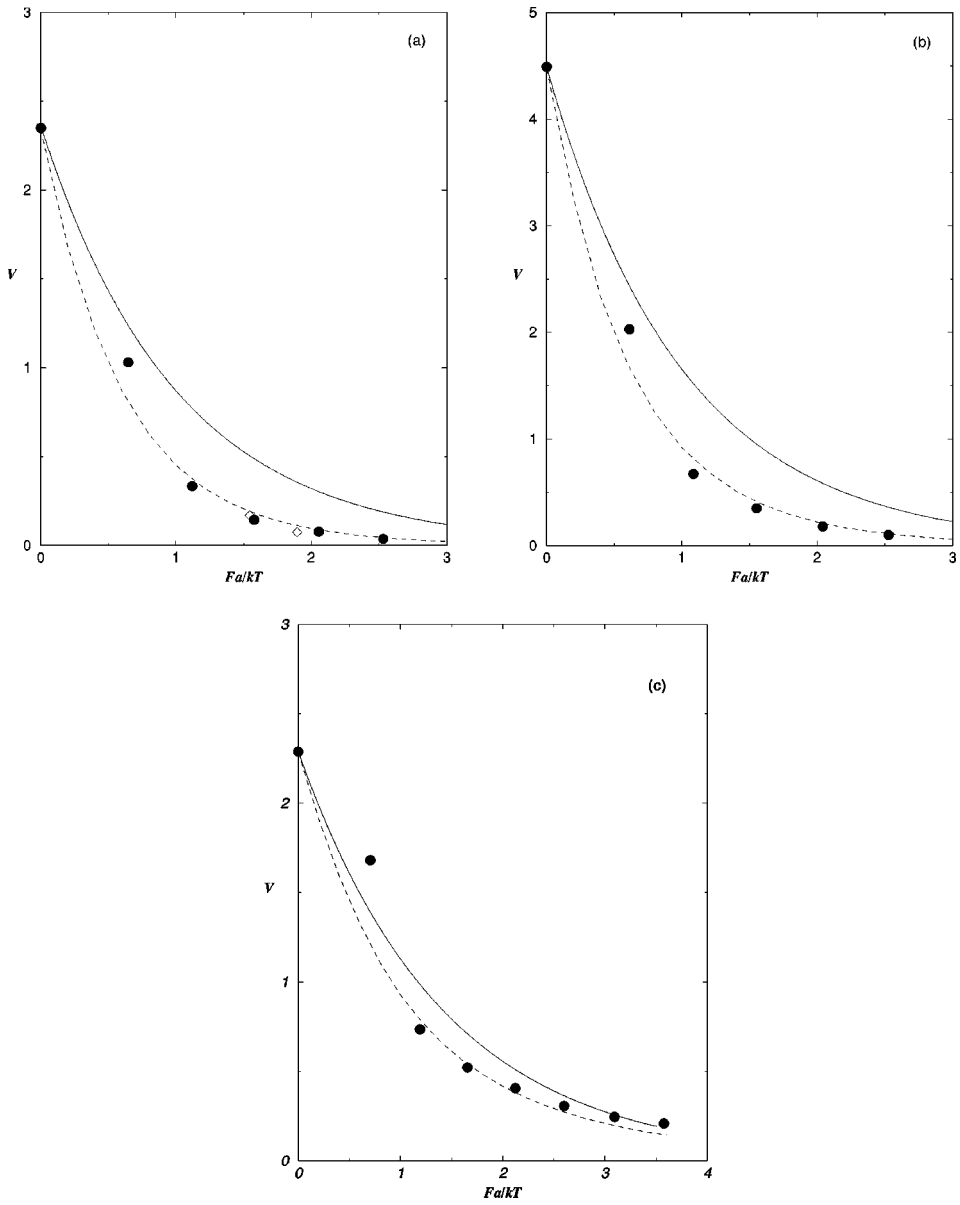

FIG. 4. Growth rates (solid circles) vs the total force F. (a) Hard force field, perpendicular incidence. (b) Soft force field, perpendicular incidence. (c) Hard force field, 45° incidence. Rates are given in units of μkTc, where μ is the monomer mobility and c is the concentration. Force is given in units of a/kT. The solid line corresponds to exponential decay [cf. Eq. (1)]. Diamonds in (a) correspond to the mobility enhanced by a factor of 2 (left) and reduced by a factor of 10 (right). Dashed curves correspond to the theory of Eq. (12).

factor of $1/\sqrt{2}$. Thus the thermal-ratchet prediction [13] for this case is $v \propto \exp(-Fa/\sqrt{2}kT)$. It is seen that the corrections to the exponential dependence are much smaller for oblique incidence than for $\theta_i = 0$. The largest discrepancies are about 30% in the range $Fa/kT = 1$ to 1.5. The decay rate at the highest force values actually seems to be slower than that in the exponential curve. We believe that this is caused by two factors. The first is that, as will be discussed below, there is a non-negligible probability of monomer addition even below the critical height for the obstacle. The second is bending of the filament as a result of the applied forces. For example, at $Fa/kT = 2.5$, we find that the tip of the fiber at the end of the growth process (when it is 36 monomers long) is bent about 15° relative to the 45° angle at the base. The bending is proportional to the square of the fiber length, and the observed velocities correspond to a weighted average of the bending between long and short fibers. The filament bending is expected to cause the growth rate to increase since the projection of the applied force on the growth axis becomes smaller, and also diffusion to the tip becomes less restricted. (We are plotting the monomer addition rate, not the rate of growth in the z direction.) We have in fact observed that the growth rates become larger for longer fibers. This may be partly due to such bending effects, and partly due to the fluctuations of the fiber tip. The latter may be estimated in terms of the effective elastic modulus of the fiber tip. As defined by Mogilner and Oster [15], the modulus is $\kappa = 4\lambda kT/l^3 \sin^2 \theta_i$, where λ is the persistence length and l is the length of the fiber. The rms vertical fluctuation of the fiber tip is then $\sqrt{kT/\kappa}$. With the persistence length of

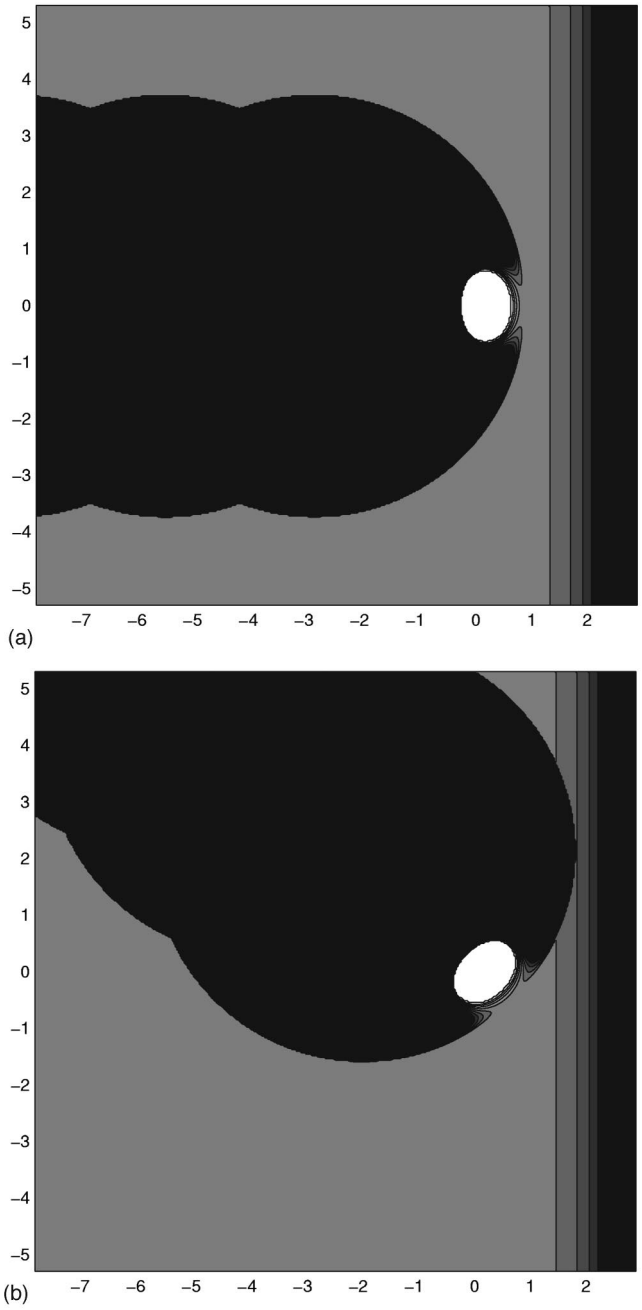

FIG. 5. Energy contours for a monomer approaching a fiber tip with a hard force field, in the presence of an obstacle. Contours are as in Fig. 1. (a) Perpendicular incidence. (b) 45° incidence.

2650 monomers resulting from the hard force field, we find that the rms vertical fluctuation exceeds the monomer size at a fiber length of 17 monomers.

B. Interpretation

We believe that the corrections seen in the perpendicular incidence case [Figs. 4(a) and 4(b)] result from the restriction of monomer diffusion to the fiber tip by the impinging obstacle. Such restriction will occur even when the obstacle is elevated by a distance a or more. Figure 5(a) shows energy contours for a monomer approaching a tip oriented perpendicular to the obstacle, when the obstacle is elevated a distance $1.25a$ relative to its equilibrium position for $Fa/kT=1.0$. The contours are at integer multiples of kT. The easily accessible paths corresponding to energies less than kT are confined to a narrow band by the presence of the obstacle. This is expected to slow the diffusion to the tip. Effectively, the monomers must travel through a tunnel in order to get to the basin of attraction near the tip. Another possible explanation for the observed effect would be that even in the region with energy less than kT, there is a finite energy from the interaction with the obstacle. However, this energy is proportional to the the length scale of the interaction between the obstacle and the monomers. In a few cases, we have made this length scale five times smaller, and the velocities are unchanged to within a few percent. Therefore, this monomer-obstacle interaction energy does not seem to be the major factor, but rather the blocking effects of the obstacle. In the oblique incidence case [cf. Fig. 5(b)], the obstacle is at a height of a $a(1/\sqrt{2}+0.25)$ since in the thermal-ratchet model an elevation of only $a/\sqrt{2}$ is required to allow a new monomer in. Here, one sees that the diffusion paths are fairly unrestricted, and the corrections should be small as observed.

To make this physical picture more precise, we have calculated the velocities for model fiber configurations in which the obstacle is held at a fixed distance from the fiber tip. The results are shown in Figs. 6(a)–6(c) for the hard and soft force fields, respectively, at perpendicular incidence, and the hard force field at 45° incidence. The edge of the obstacle is defined as the point where the monomer-obstacle interaction energy is equal to kT. Thus when $Z=0$, the interaction energy of the last monomer in the fiber with the obstacle is kT. For perpendicular incidence, the velocity at $Z/a=1$ is nearly zero for both force fields; the velocity comes within 20% of the free-growth velocity only for $Z/a>2$. For 45° incidence, the velocity is a quarter of the free-fiber value already at $Z/a\cos 45°=1$, and the velocity is appreciable even for values of Z less than this critical value. These results are expected on the basis of the energy contours in Fig. 5.

The appropriate generalization of Eq. (1) is then the following:

$$v(F)=\int_0^\infty v(Z)P(Z,F)dZ, \tag{12}$$

where F is the force, Z is the obstacle position, and $P(Z,F)=(\text{const})\exp(-E/kT)$ is the probability of a certain value of Z. Here the obstacle-fiber interaction energy is $E=W_2(z-Z)+FZ$, where z is the z coordinate of the last monomer in the fiber. Equation (12) reduces to Eq. (1) if $v(Z)$ has the form of a step function beginning at a $Z=a$, and W_2 is sufficiently short ranged. The dashed lines in Figs. 4(a)–4(c) correspond to a numerical evaluation of Eq. (12). For all three cases, the agreement with the simulation results is quite close, with the largest discrepancies of about 30% occurring for small but nonzero forces. Thus the gradual rise of the velocity seen in Figs. 6(a)–6(c), as opposed to an abrupt jump, is at the heart of the observed effect for perpendicular incidence. We note that for 45° incidence, the nonnegligible velocities in Fig. 6(c) for $Z<a\cos 45°$ will, according to Eq. (12), lead to a reduced decay rate in the force-velocity relation. This was indeed seen in Fig. 4(c).

As noted above, in the case of 45° incidence, substantial fluctuations occur in the position of the filament tip, exceed-

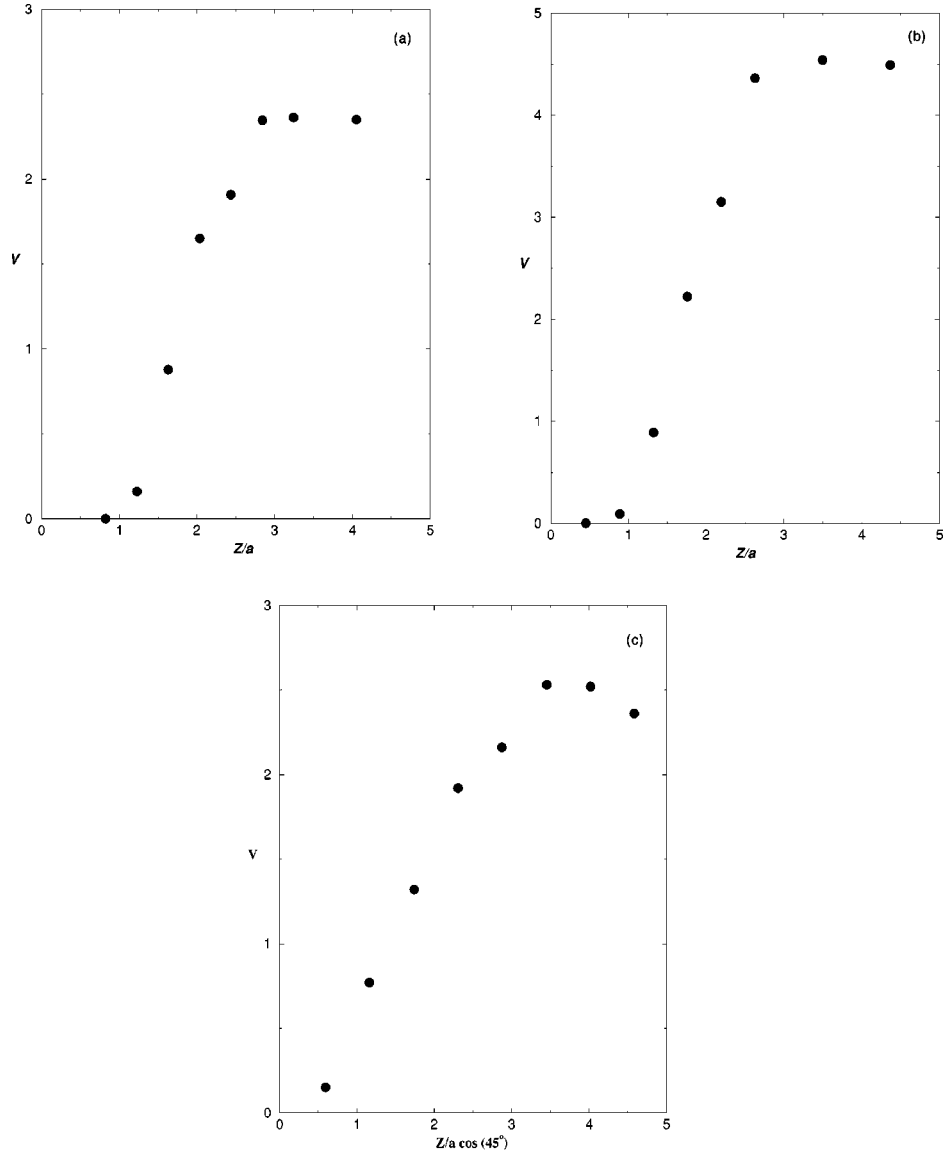

FIG. 6. Fiber growth rates with fixed tip-fiber spacing. (a) Hard force field, perpendicular incidence. (b) Soft force field, perpendicular incidence. (c) Hard force field 45° incidence. Z is measured relative to the point at which the tip-fiber interaction energy is kT. Rates are given in units of $\mu kT/c$, where μ is the monomer mobility and c is the concentration.

ing one monomer size by the time the filament has reached a length of 17 monomers. These are naturally included in the simulations. However, we feel that the fluctuations are not the crucial effect in the difference between the perpendicular and 45° cases. As summarized in Eq. (12), the important factor in determining the velocity is the distribution $P(Z,F)$ of distances between the monomer and the tip. Regardless of fluctuations, the fiber is still exerting an average force of F on the obstacle, and vice versa. Therefore, $P(Z,F)$ will still decay exponentially with Z. On the other hand, if the obstacle were so much less mobile that the time for it to fluctuate a distance a from the tip exceeded the time for a monomer to diffuse to the basin of attraction, then the membrane fluctuations would become the determining factor.

IV. SENSITIVITY OF RESULTS TO SIMPLIFICATIONS OF THE MODEL

The calculations described above make a number of simplifying assumptions. The major ones are the use of two- instead of three-dimensional simulations, and the choice of *ad hoc* forms for the monomer-monomer and monomer-fiber interactions. In this section we address the likely errors arising from these simplifications.

A. Dimensionality

In order to get an idea of how much the results obtained here would carry over to a three-dimensional calculation, we analyze a simplified diffusion model. The basic idea of this model is that the ''tunnels'' that the monomers must pass through, either on the left or the right, to get to the basin of attraction, provide a diffusion resistance R_{tunnel}. This resistance is defined as the ratio of the concentration difference between the ends of the tunnel and the current flowing through the tunnel. A key physical parameter is then the ratio $\eta = R_{\text{tunnel}}/R_{\text{free}}$, where R_{free} is the diffusion resistance associated with the motion of monomers from the edge of the simulation region to the basin of attraction in the absence of

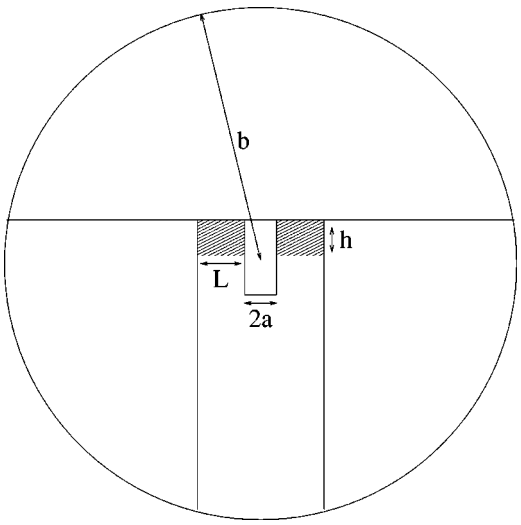

FIG. 7. Schematic rendering of the diffusion model.

the obstacle. If η is large, then the effects of the obstacle on the rate of diffusion of monomers to the fiber tip will be correspondingly large.

To evaluate R_{tunnel} in two dimensions, we model the tunnels as shown in Fig. 7. Each is a strip (shaded in the figure) of height h and length L, leading to the basin of attraction, which has width $2a$. The height h corresponds to the width of the path available for monomer diffusion to the tip, when the tip elevation exceeds the minimum value of a by a small amount δz. Roughly speaking, δz would correspond to h. One readily shows that in this geometry, $R_{\text{tunnel}}=L/2Dh$, where D is the diffusion constant. (Note that the factor of two in the denominator comes from the fact that there are two tunnels supplying currents in parallel.) In three dimensions, we use a torus geometry for the tunnel, with height h, outer radius $L+a$, and inner radius a. In this case one obtains $R_{\text{tunnel}}=\ln(L/a+1)/2\pi Dh$. To evaluate R_{free} we model the basin of attraction as a disk in two dimensions and a sphere in three dimensions, the radius in each case being a. The source of current is a circular or spherical boundary with radius b. For these cases, standard calculations [22] give $R_{\text{free}}=\ln(b/a)/2\pi D$ in two dimensions and $R_{\text{free}}=(1-a/b)/4\pi aD$ in three dimensions. We thus obtain

$$\eta^{2\text{D}}=\pi L/h\,\ln(b/a) \tag{13}$$

and

$$\eta^{3\text{D}}=2a\,\ln(L/a+1)/h(1-a/b). \tag{14}$$

These parameters roughly describe the reduction of the velocity by the restricted-diffusion effects near the fiber tip. We do not have precise estimates of them, but we can very roughly estimate them on the basis of the energy contours. In the perpendicular-incidence case, Fig. 5(a) would suggest a value of 1 nm for L as the distance over which the tunnel size is constant, and a value of 0.5 nm for h as the separation between the tip and the first energy contour. The parameter b has the value 6.75 nm used in the simulations. A value of 0.5 nm for a is obtained by fitting R_{free} to our simulation velocities in the absence of the obstacle, and is also consistent with the size of the white attraction region in Fig. 5(a). Using these values gives an estimate of 2.5 for $\eta^{2\text{D}}$, which in the simplest analysis would correspond to an increase in the diffusion resistance by a factor of 3.5, commensurate with the observed velocity reductions at high forces. At oblique incidence, Fig. 5(b) would suggest a much larger value of h, leading to a much smaller value of $\eta^{2\text{D}}$, again consistent with the simulation results.

The ratio of the strength of the effect in three dimensions to that in two dimensions is then given by

$$\eta^{3\text{D}}/\eta^{2\text{D}}=2a\,\ln(L/a+1)\ln(b/a)/\pi L(1-a/b). \tag{15}$$

Using the above values of the model parameters, we obtain an estimate of 0.98 for $\eta^{3\text{D}}/\eta^{2\text{D}}$ at perpendicular incidence, indicating that the dimensionality effects are not too strong. This result is more sensitive to the value of L than to a. Halving or doubling L changes η^{3D}/η^{2D} to 1.24 and 0.72, respectively. Increasing or reducing a by a factor of two changes η^{3D}/η^{2D} only very little, to 0.99 and 0.88, respectively. In any case, for a large variation of parameter values, the magnitude of the effect in three dimensions is quite comparable to that in two dimensions.

B. Monomer-monomer interactions

The greatest simplification made in our interaction model is that the filament is treated as a straight line of monomers, whereas in actin filaments the monomers attach on alternating sides of the fiber, and in microtubules they are arranged in a spiral. This precludes quantitative comparison with data for these systems. As pointed out in Sec. III, however, the main feature determining the strength of the effects found here is the orientation of the top of the fiber relative to the plane of the obstacle. Thus the correction terms that are found here will be important to the extent that, during the process of fiber growth, configurations are encountered in which the top of the fiber tip is parallel to the obstacle. This could occur, for example, in the growth of actin fibers away from perpendicular incidence, at angles where the plane determined by the two monomers at the tip is parallel to the obstacle. It can also occur in principle if a flexible membrane ''drapes'' itself over the face of the fiber even if this face is not parallel to the average orientation of the obstacle. However, membranes will usually be too stiff for this effect to be important. Typical values [23] for the bending moduli κ of lipid bilayers are on the order of 10^{-19} J. The radius of curvature R for bending induced by a filament exerting a force F on a membrane would be roughly κ/F. Using typical forces of 10^{-12} N or less generated by the growth of biological filaments, we obtain $R=100$ nm, considerably larger than the size of a monomer. Over the cross section of a monomer, only very small effects of membrane bending would then be observed.

The aspect of the monomer-monomer field that affects the results most strongly is the potential-energy surface for a monomer approaching the tip, as seen for example in Figs. 1 and 5. The precise form of this surface chosen here is of course *ad hoc*. Nevertheless, the general form of the variation of the energy surface is likely correct. A monomer residing in its preferred position at the tip of the fiber will have a substantial barrier to sideways motion, as indicated by the

long persistence lengths of actin filaments and microtubules. Extending the effective elastic modulus defined by Mogilner and Oster [15] to define a spring constant for the sideways motion of a single monomer, the basis of these persistence lengths l, one obtains $\kappa_{eff}=4lk_BT/a^3$, where a is the monomer size. For actin fibers, using a value of 7μ for the persistence length [19], and $a=2.7$ nm, one finds that $k_{eff}\delta x^2=k_BT$ for $\delta x=0.05$ nm. This corresponds to a very rapid variation of the energy in the vicinity of the minimum, as we obtain here. The major feature of the force field entering the simulations is the width of the ''funnel'' leading to this minimum. We are not able to establish this width precisely. However, we feel that a value much greater than 3.5 nm, the value for the soft force field obtained visually from Fig. 1(b), is unrealistic. Comparing the observed fiber growth rate of 100 monomers/sec at a monomer concentration of 10 μM and a diffusion constant of $(3-6)\times10^{-12}$ for actin monomers in the cell cytoplasm [24], one obtains, according to diffusion-limited reaction-rate theory [25], a classical reaction radius of about 0.3 nm. We feel that this precludes a basin of attraction size exceeding this by more than an order of magnitude. In sum, we believe that the most physically reasonable range of possibilities for the shape of the potential-energy profile near the fiber tip is spanned by the present calculations.

It is possible for long-ranged electrostatic interactions between the monomers and the tip to be present, and these are excluded from the present model. Such interactions would induce a slowly varying potential field around the fiber tip. The main effect of such a potential field would be to increase or decrease the local density of monomers. This would affect the absolute velocities of the growth velocity, but would not change the ratio of the velocity at a finite force to that at zero force.

C. Monomer-obstacle interactions

The key parameter in the interaction between the monomers and the obstacle is the length range of the interaction potential. The magnitude of the prefactor in front of the exponential will not affect the results, since the position of the sheet will adjust itself to achieve a position where the force from the monomers on the obstacle cancels the applied force, and the energy at this point is determined entirely by the applied force and the length scale of the interaction potential. In the direction of ''harder'' interaction potentials the results do not seem to be sensitive to the length scale of the interactions. As mentioned above, reducing this length scale by a factor of five changed the simulation velocity by only a few percent. The effects of potential long-ranged contributions to the monomer-obstacle interactions depend on the sign of these contributions. If they are attractive, they will change the local monomer concentration and thus the absolute magnitude of the velocity, but will not change the form of the dependence of the velocity on applied force since the energy changes from displacements on the order of a will be dominated by the hard repulsive component of the interaction potential.

However, if long-ranged repulsive interactions are present, the scenario can become quite different. These interactions will determine the energy required to displace the obstacle relative to its equilibrium position r_0 for a given force F, as well as the energy required to bring a monomer up to the obstacle. One readily shows that for a displacement Δr small in comparison with $\kappa_{\rm obst}^{-1}$ the energy change is $\Delta E(\Delta r)=1/2F\kappa_{\rm obst}\Delta r^2$, so that the energy change of lifting the obstacle to a height a becomes

$$\Delta E(a)=Fa(\kappa_{\rm obst}a/2). \tag{16}$$

For a slowly varying force field, $\kappa_{\rm obst}a<1$, so that the energy required to raise the obstacle is greatly reduced. However, because of the long range of the interaction, an energy is required to bring the monomer up to the obstacle. This is given approximately by $F/\kappa_{\rm obst}$, which could exceed Fa by a substantial amount. The net effect of these two contributions is a more rapid decay of the force-velocity relation, and possibly corrections greater than those obtained here.

Another important physical effect that is missing from the present simulations is the flexibility of the obstacle as is present in, for example, membranes. This flexibility has two main effects: it results in lateral fluctuations so that at a given time, the obstacle is not flat, and it can cause the membrane to ''drape'' itself around the fiber at high forces. We see no straightforward way of establishing the importance of the lateral membrane fluctuations in the present calculations. However, in view of the large values of the bending rigidity alluded to above, in comparison with kT, we believe that these fluctuations are not a major factor. As mentioned above, the ''draping'' effect is likely very small for biological filament growth. It is, however, very possible [26] that the fibers are attached to the membrane rather than floating freely relative to it. Evaluating the importance of such effects would require a plausible model for the attachment mechanism, and these mechanisms are poorly understood at present.

V. CONCLUSIONS

The above results indicate that over most of the ''phase'' space of fibers growing against membranes, the exponential form (1) for the force velocity relation is accurate to within 30%. However, in cases where diffusion to the basin of attraction is limited either because the monomer faces are parallel to the obstacle, one should expect substantial corrections to the simple exponential form (1). This could potentially explain some of some of the discrepancies pointed out in connection with the measured force-velocity relation of Ref. [12]. However, our knowledge of the geometry at the point where the fiber interacts with the obstacle is not precise enough to establish the importance of the diffusion-rate effects and whether they exceed the subsidy effects discussed in Ref. [17].

These conclusions should be useful in explaining the basic physics of motion based on actin polymerization. For actin fibers pushing a membrane at perpendicular incidence, the face of the growing fiber is not parallel to the membrane, since the monomers alternately attach to different sides of the fiber. At any given time, the face of the fiber then forms an angle of about 45° to the plane of the membrane, indicating that the results in Fig. 4(c) should be the most relevant.

Thus the exponential behavior should be correct. The corrections could potentially be important in a narrow range of orientations in which the face of the fiber (during half of the steps) is parallel to the membrane. If the fiber grows at an angle of 45°, the orientation of the fiber surface will alternate between 0° and 90° relative to the membrane. One could then expect substantial slowing in the steps which correspond to 0°. In these cases, the fiber itself will also be fluctuating, but as argued above this will not have a large effect on the velocity unless the obstacle is very immobile.

Having more confidence in the force-velocity relation should enhance the reliability of actin-growth simulations performed with coarser models. Such simulations can treat a large number of actin fibers impinging on a membrane, or even the whole assembly impinging on an intracellular pathogen. For example, in a recent study van Oudenaarden and Theriot [27] have simulated the propulsion of plastic beads in cell extracts with a model based on a number of fibers exerting forces on the beads. In their simulations, an assumed form is taken for the probability of the monomer addition to a fiber in terms of the time-averaged position of the fiber relative to the bead, or equivalently, the force acting between the two. A better knowledge of the relationship between the force and the monomer addition rate can help pin down the validity of the assumptions underlying such simulations. To the extent that the restricted-diffusion effects are important, they should have noticeable effects on the structure of membranes that are being pushed forward by collections of actin fibers. As a result of random fluctuations, some fibers will eventually get ahead of others, and these will be exerting larger forces on the membrane. If the velocity drops off rapidly with the force, then these fibers will be slowed down significantly. This will result in the membrane surface being smoother than otherwise expected. Future work should treat such many-fiber effects, and also explore the effects of fiber growth angle and branching.

ACKNOWLEDGMENTS

I am grateful to John Cooper for stimulating my interest in this project, and to Jonathan Katz and Elliot Elson for useful conversations. This research was supported by the National Institutes of Health under Grant No. GM38542-12.

[1] T. Pollard, J. Cell Biol. **103**, 2747 (1986).
[2] J. A. Cooper, Annu. Rev. Physiol. **53**, 585 (1991).
[3] J.-B. Marchand *et al.*, J. Cell Biol. **130**, 331 (1995).
[4] V. Argiro, M. Bunge, and J. Johnson, J. Neurosci. Res. **13**, 149 (1985).
[5] S. Felder and E. L. Elson, J. Cell Biol. **111**, 2513 (1990).
[6] L. G. Tilney and D. A. Portnoy, J. Cell Biol. **109**, 1597 (1989).
[7] A. S. Sechi, J. Wehland, and J. V. Small, J. Cell Biol. **137**, 155 (1997).
[8] L. A. Cameron, M. J. Footer, A. van Oudenaarden, and J. A. Theriot, Proc. Natl. Acad. Sci. U.S.A. **96**, 4908 (1999).
[9] T. P. Loisel, R. Boujemaa, D. Pantaloni, and M.-F. Carlier, Nature (London) **401**, 613 (1999).
[10] V. C. Abraham, V. Krisnamurthi, D. L. Taylor, and F. Lanni, Biophys. J. **77**, 1721 (1999).
[11] C. Rotsch, K. Jacobson, and M. Radmacher, Proc. Natl. Acad. Sci. U.S.A. **96**, 921 (1999).
[12] M. Dogterom and B. Yurke, Science **278**, 856 (1997).
[13] C. S. Peskin, G. M. Odell, and G. F. Oster, Biophys. J. **65**, 316 (1993).
[14] T. L. Hill, *Linear Aggregation Theory in Cell Biology* (Springer-Verlag, New York, 1987), Chap. 2.
[15] A. Mogilner and G. Oster, Biophys. J. **71**, 3030 (1996).
[16] A. Mogilner and G. Oster, Eur. Biophys. J. **25**, 47 (1996).
[17] A. Mogilner and G. Oster, Eur. Biophys. J. **28**, 235 (1999).
[18] M. Doi and S. F. Edwards, *The Theory of Polymer Dynamics* (Clarendon Press, Oxford, 1998), Chap. 3.
[19] D. Riveline, C. H. Wiggins, R. E. Goldstein, and A. Ott, Phys. Rev. E **56**, 1330 (1997).
[20] In order to avoid an excessive number of excursions back and forth across the circle radius, the added monomer is placed a small distance inside *R*.
[21] In two dimensions, the time for a particle to diffuse to capture is not strictly proportional to the area of the region in which it diffuses, but contains logarithmic corrections. Therefore the calculated velocities are not strictly independent of *R*. I have verified by use of a few test cases with larger values of *R* that the predicted logarithmic scaling is observed. Extrapolating to a value of *R* corresponding to a physiological interparticle spacing for actin monomers would modify the calculated velocities by a constant factor of about two, which we have not included because our focus is the force dependence of the velocity rather than its absolute magnitude.
[22] H. C. Berg, *Random Walks in Biology* (Princeton University Press, Princeton, New Jersey, 1993).
[23] U. Seifert and R. Lipowsky, in *Structure and Dynamics of Membranes*, edited by R. Lipowsky and E. Sackmann, Handbook of Biological Physics, Vol. 1A (Elsevier, New York, 1995), pp. 403–463.
[24] J. L. McGrath *et al.*, Biophys. J. **75**, 2070 (1998).
[25] M. Daune, *Molecular Biophysics: Structures in Motion* (Oxford University Press, New York, 1999), Chap. 8.
[26] D. J. Olbris and J. Herzfeld, Biochim. Biophys. Acta **1495**, 140 (2000).
[27] A. van Oudenaarden and J. A. Theriot, Nat. Cell. Biol. **1**, 493 (1999).